Study of Metal-Carboxylate Complex from Pinus Elliottii Resin Applied as Antibacterial Pigment

Jamille Correa[1], Cristina Zanette[1], Fauze Anaissi[1], Peter Guttmann[2], Stephan Werner[2], Carla Bittencourt [3,a)]

[1] *Department of Chemistry, Universidade Estadual do Centro-Oeste, UNICENTRO, Guarapuava, Paraná, Brazil.*
[2] *Department X-ray microscopy, Helmholtz-Zentrum Berlin für Materialien und Energie GmbH, Berlin, Germany.*
[3] *Chimie des Interactions Plasma Surface, CIRMAP, Université de Mons, Place du Parc 23, 7000, Mons, Belgium.*

[a)]Corresponding author: *carla.bittencourt@umons.ac.be*

Abstract. Metal carboxylate complexes derived from Pinus elliottii resin have been reported as promising pigments for paints and coatings due to their high antibacterial, antifungal, and antiviral properties. Besides the antibacterial and/or antiviral properties of the pigments, color, and stability are essential characteristics often associated with the oxidation state of the coordinating metal atom, such as Mn, Fe, Co, Ni, or Cu. However, using traditional analysis techniques, the low metal concentration in the pigment makes it challenging to determine the metal oxidation state and the electronic structure of the metal complex used as pigments. To this aim, we use nanoscale NEXAFS recorded at the XM-beamline (U41-PGM1-XM) at BESSY II to investigate the local electronic structure surrounding a selected elemental species its oxidation state. The design of the X-ray Microscopy Beamline U41-PGM1-XM enables analysis in the soft (0.25 keV – 1.5 keV) and tender X-ray photon energy regime (1 keV - 2.7 keV), allowing the study via Near Edge X-ray Absorption Fine Structure of different metal carboxylate complexes used as pigments.

INTRODUCTION

Pigments have the function of imparting color, opacity, and mechanical rigidity to paints and coatings. In addition, they can have functional properties, such as antibacterial, antiviral, and antifungal. In this context, research on antibacterial coatings has been supported by the paint industry for applications on both indoors and outdoors in hospitals, schools, nursing homes as well as daycare centers to reduce the risk of infections in these environments where the bacterial population tends to be very high [1]. Among the studied materials, metal carboxylate complexes derived from Pinus elliottii resin (part of the natural defense mechanism against herbivores and pathogens of pine trees) have been reported as promising pigments for paints and coatings due to their high antibacterial, antifungal, and antiviral properties [2]. In addition to these properties, color and its stability are important pigment characteristics often associated with the oxidation state of the coordinating metal atom as Mn, Na, Nd, Fe, Co, Ni, or Cu. [3,4] The low metal concentration in pigments makes it difficult to determine the metal oxidation state and the electronic structure of the metal complex using traditional analysis techniques. To this aim, Near Edge X-ray Absorption Fine Structure (NEXAFS) spectroscopy recorded in the transmission mode is a powerful technique for studying the local electronic structure surrounding a selected elemental specie and its oxidation state. The oxidation state is an essential quantity because the distribution of electron/charge density in complexes determines their chemical, physical and biological functions/properties and color. Certain chemical elements can have different oxidation states and, thus, different chemical properties. For example, manganese (Mn) can be found in MnII to MnVII oxidation states covering electron configurations from $3d^5$ to $3d^0$, and nickel (Ni) can have Ni0 to NiIV covering $3d^{10}$ to $3d^6$. In contrast, copper can have CuI and CuII oxidation states. In material chemistry, the

Proceedings of the 15th International Conference on X-ray Microscopy – XRM2022
AIP Conf. Proc. 2990, 020014-1–020014-8; https://doi.org/10.1063/5.0168172
Published by AIP Publishing. 978-0-7354-4672-4/$30.00

determination of the oxidation states, i.e. the measured number of electrons/holes localized in the bonding orbital, has helped in understanding the chemical and biochemical roles of many metal sites, while unresolved oxidation states have contributed to longstanding controversies in many systems [5,6]. Here we study the electronic structure of the coordinating metals (Mn, Fe, Co, Ni, and Cu) in M-abietate complexes using near-edge X-ray absorption fine structure spectromicroscopy (NEXAFS). We use nanoscale NEXAFS recorded at the transmission X-ray microscopy (TXM) beamline (U41-PGM1-XM) to investigate the local electronic structure surrounding a selected elemental specie and its oxidation state. The TXM optical design combines a spectral resolution of $E/\Delta E = 1 \times 10^4$ with a spatial resolution of 25 nm in a field of view of 15–20 μm and a data acquisition time of ~ 6 s per image. The NEXAFS-TXM technique has the advantage that one image stack visualizes a large number of nanostructures, which allows the evaluation of sample homogeneity and already contains statistical information [7]. The design of the X-ray microscopy beamline U41-PGM1-XM provides analysis in the soft (0.25 keV – 1.5 keV) and tender X-ray photon energy regime (1 keV - 2.7 keV).

The relative amount of metal in the complexes was evaluated by X-ray photoelectron spectroscopy (XPS). The different colors of the product indicate the effective doping during the proposed synthesis route. The antibacterial activity of the Mn-carboxylate complex will be discussed.

MATERIALS AND METHODS

Synthesis of the pigments

The metal-carboxylates studied here were obtained from Pinus elliottii resin using a green synthesis route (scheme 1) and applied as an antibacterial pigment. First, the Pinus resin is purified and then dissolved in water with sodium hydroxide (NaOH, P.A.) mixed in a molar proportion of 1:1 under mechanical stirring for 3 hours at 90 °C until the formation of a hygroscopic salt (Na-abietate). The H_2O evaporates in this step. Next, the synthesized Na-abietate and a metal sulfate are separately dissolved in water. Then, these solutions are mixed dropwise in the molar proportion of 3:1 (Na-abietate: M+). In this step occurs the formation of the complex M-abietate (M: Mn, Fe, Co, Ni, or Cu). Finally, the complex is washed out with deionized water and filtered, dried in an oven at 70 °C for 5 hours, and macerated in an agate mortar and pestle. The product is a powder with a color depending on the doping atoms and their oxidation state. More details about the synthesis can be found in [2].

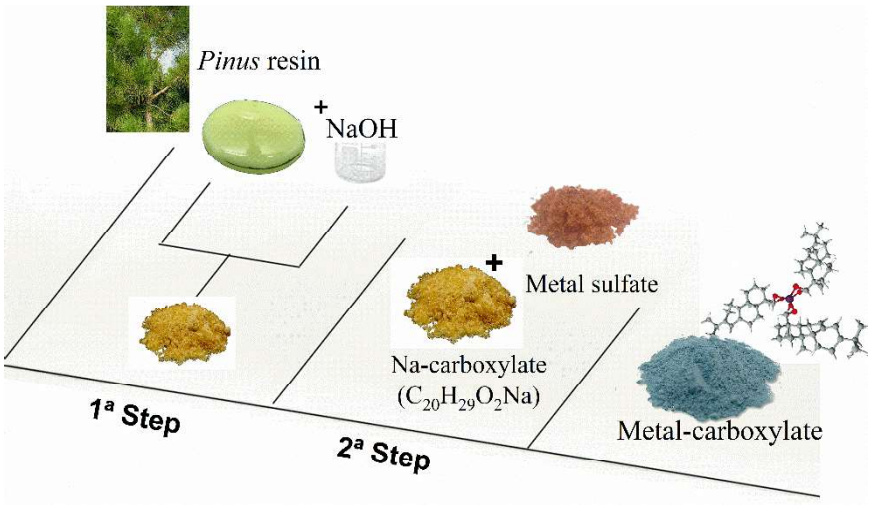

SCHEME 1. Route for obtaining Metal-carboxylate. In the first step, purified Pinus resin is used to obtain Na-abietate. Next, in the second step, the synthesized Na-abietate and a metal sulfate are mixed under selected conditions to obtain metal-carboxylate.

The relative atomic elemental composition of the samples was evaluated by X-ray photoelectron spectroscopy (XPS). A VersaProbe PHI 5000 spectrometer from Physical Electronics, equipped with a monochromatic Al Kα X-

ray source with an energy resolution of 0.5 eV and X-ray beam diameter of 200 μm, was used to record the XPS spectra. During the measurements, a dual-beam charge neutralization with an electron gun (1 eV) and an Ar ion gun (≤10 eV) was used for charge compensation of the sample surface. The C1s peak centred at 284.6 eV was used for binding energy reference. For XPS analysis, the powder was pressed to a pellet and supported on a double-face conductive tape compatible with XPS.

The most direct way of measuring NEXAFS spectra is to perform a transmission measurement. The transmission X-ray microscope (TXM) end-station equipped with a 25 nm zone plate installed at the undulator beamline U41-PGM1-XM at the electron storage ring BESSY II, Helmholtz-Zentrum Berlin (HZB) was used to record the NEXAFS spectra. The calculated spectral resolution was $E/\Delta E = 20000$. The photon flux variation with photon energy (hv) and acquisition time used for recording the different regions of the spectra was corrected using a spectrum recorded in bare areas near the region of interest (ROI). The analysis software package aXis2000 which was initially written for STXM data analysis can also handle the HZB TXM data sets. Therefore, this software was used for data analysis (A.P.Hitchock, http://unicorn.mcmaster.ca/aXis2000.html) (accessed on 10 March 2021). For the NEXAFS-TXM analysis, the samples were dispersed in ethanol by ultrasonication and dropped on a holey lacey carbon membrane supported on 300-mesh copper grids. Ethanol was then evaporated at room temperature, and the image stacks were recorded.

The antibacterial activity of Mn-abietate was evaluated against Staphylococcus aureus bacteria (ATCC 6538P) using the methodology by JIS (Japanese Industrial Standard) Z 2801:2010 [8]. The complex was dispersed in a concentration of 10 % (w/w) in industrial paint for the tests. The cardboard disc specimens with 5.0 cm^2 were cleaned with 70% ethanol solution and dried according to the standard procedure. Discs painted only with white commercial paint were also tested (control). According to the Japanese Standard, the number of viable bacteria in the control and the test samples are compared after exposure for 24 h. The number of bacteria colonies was compared using the R factor, corresponding to the decimal logarithm of the rate of the bacteria concentrations between the reference (specimens with commercial white paint only) and the samples. A material presents antibacterial activity when this R factor value is ≥2 log reduction.

Experimental Characterization

The samples were first analyzed by X-ray photoelectron spectroscopy. Table 1 shows the evaluated relative atomic concentration. Unfortunately, the relative amount of the metal in the M-carboxylates is low. Therefore, from XPS analysis, the evaluation of the oxidation state is not straightforward.

Samples	C	O	Na	S	Mn	Fe	Co	Ni	Cu
Na-carboxylate	52.1	31.1	15.8	1.0	-	-	-	-	-
Mn- carboxylate	80.5	16.5	0.4	1.4	1.2	-	-	-	-
Fe- carboxylate	81.5	13.3	1.8	0.5	-	2.9	-	-	-
Co- carboxylate	77.8	17.2	1.2	0.3	-	-	3.5	-	-
Ni- carboxylate	82.7	14.3	1.0	-	-	-	-	2.0	-
Cu- carboxylate	78.9	14.6	3.3	1.3	-	-	-	-	1.9

TABLE 1: Relative concentration (at.%) of elements according to X-ray photoelectron spectroscopy (XPS) analysis. Na and S contamination are related to the precursors used in the synthesis.

Figure 1 shows typical X-ray images of an image stack used to record a NEXAFS spectrum. For absorption spectroscopy, it is necessary to measure two spectra: one spectrum I(E) of transmission through the specimen or ROI and another of the incident flux $I_0(E)$. The NEXAFS spectrum is obtained as an optical density $OD(E) = -\log [I(E)/I_0(E)]$ [**7**]. A region containing a bunch of carboxylate particles was used to record the I(E) spectrum, and the I0(E) was recorded in a bare region of the sample support close to the sample region (Figure 1). The stacks have between 200 to 300 images depending on the analyzed energy range and energy step used. During the measurement, the system is kept in focus (see figure 1b). So far, nearly all absorption spectroscopy techniques cannot measure I(E) and $I_0(E)$ simultaneously, which can lead to errors in the normalization due to the instabilities of the photon beam. For nanostructures, the photon flux ($I_0(E)$) and the signal (I(E)) can be recorded in the HZB full field TXM

simultaneously at near the same position reducing the uncertainties in the normalization of the NEXAFS signal. For this, near the nanostructure, we should have a bare region (or a hole) where the $I_0(E)$ can be extracted (Figure 1). For each image, the number of photons per pixel is about 3.2*10^7; this value is under the threshold for sample damage experimentally observed during the measurements.

The number of photons per pixel is evaluated by the following equation: photon flux x condenser efficiency x exposure time x slit width x ring current). Considering the Mn edge (photon energy ~ 650 eV), the photon density: photon flux at Mn edge (around 650 eV) is 3*10^12 photons/(sec*100mA) at 20 μm exit slit [9]. Therefore the photons per pixel [10]: photon flux * condenser efficiency * exp. time * (slit width / 20 μm) * (ring current / 100 mA) = 3*10^12 * 0.8 * 6 * (15/20) * (300/100) = 3*10^13 / $(1024)^2$ = 3.2*10^7

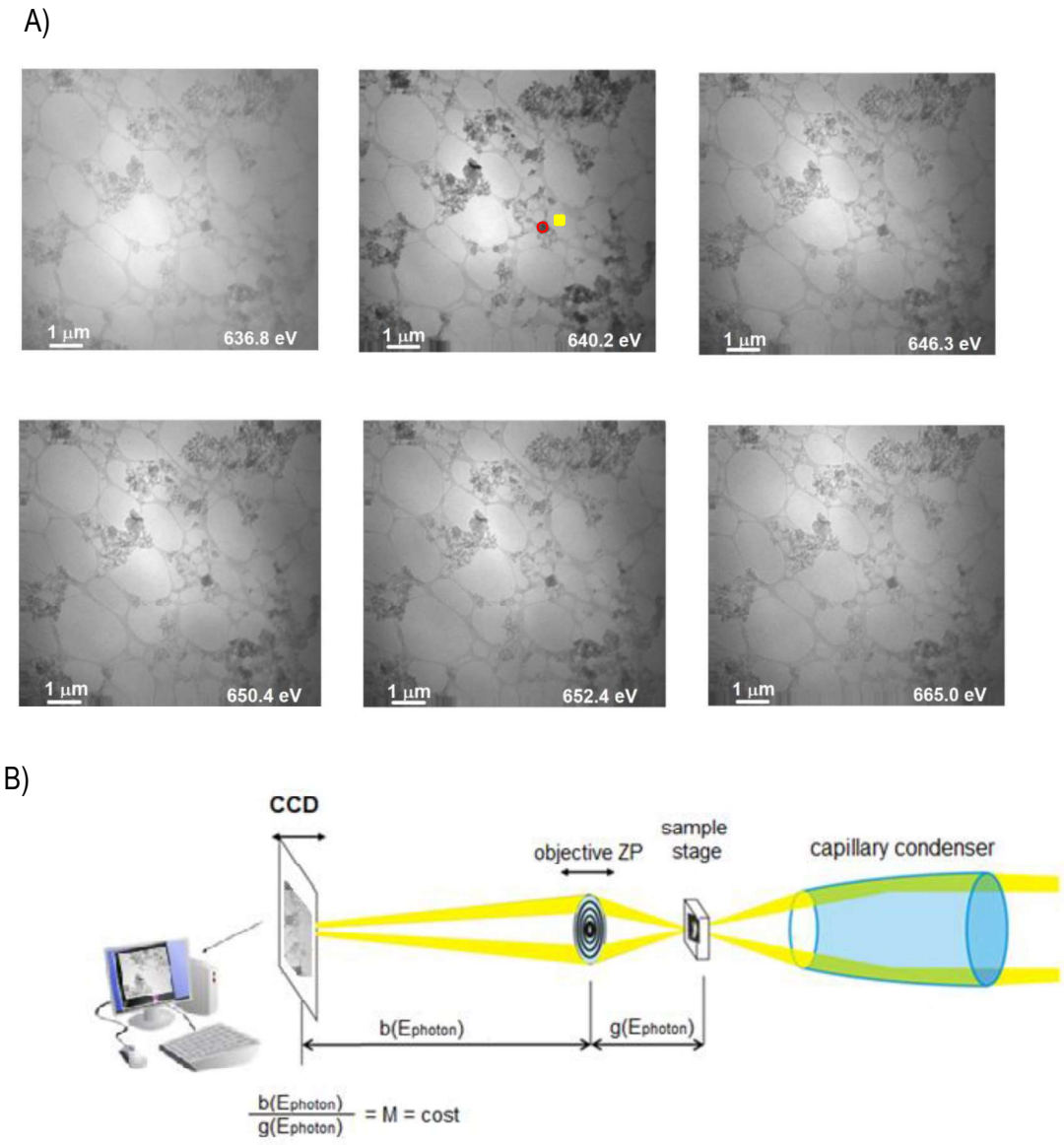

FIGURE 1. A) X-ray images at six different photon energies from an image stack recorded on the Mn-carboxylate sample at the U41 beamline using the TXM. The NEXAFS–TXM Mn L-edge (see Figure 2B) spectrum was recorded in the area delimited by the circle. The yellow square indicates the point at which the I0 was recorded. (B) Setup of the NEXAFS–TXM measurements.

RESULTS AND DISCUSSION

First, we will present the results for the Na-carboxylate precursor of the metal-carboxylate samples. The Na K-edge spectrum recorded presents three main structures (Fig. 3A). These are attributed to the excitation of a core-level electron into an unoccupied bound state [11]. The shoulder observed at 1076.9 eV is assigned to the 1s → 3p transition. The origin of the peak at 1079.4 eV is not well established. The pre-edge structure [6], was reported to correspond to the transition 1s →3s. This transition is parity forbidden in a free ion and is not observed in a NEXAFS spectrum of atomic sodium [12]. In brief, in the precursor sample, the sodium atoms are present in ionic form as expected, allowing them to be easily exchanged by metal atoms, verifying the corrected chemical reaction path with the proposed green synthesis method.

Now we turn to the analysis of the metal carboxylates after the Na substitution. The metal atoms used for the doping belong to the 3d block in the periodic table. The transition metals in the d-block are chemically characterized by exhibiting variable oxidation states, forming colored complexes, and having catalytic properties. We focus on the shape and position of the L_3-edge as it is well resolved compared to the L_2-edge. It provides information about the valence of the metal atom and hybridization of the metal and ligand orbitals in terms of the t_{2g} and e_g orbitals signatures. [5,6]. For 3d metals, a typical L-edge absorption spectrum is characterized by a pair of strong absorption peaks corresponding to $2p_{3/2}$→3d and $2p_{1/2}$→3d transitions (2p→4s is 20-fold weaker) and an invariant edge jump step between the pre-L_3 and post-L_2 regions corresponding to 2p→coninuum transitions. For manganese, the shape and position of the Mn L-edges vary with the oxidation state, Mn^{3+} and Mn^{4+} have broad L-edge features which occur at higher energy than that of Mn^{2+}. The Mn L-edge spectrum (Figure 3B) recorded on the Mn-carboxylate sample shows a broad line L3 with two edges separated by 2 eV, indicating the presence of Mn^{2+} and Mn^{3+} [5,6]. Figure 3C shows the Fe L-edge for the Fe-carboxylate sample. The Fe L_2- and L_3 edges are assigned to transitions from $2p_{3/2}$ to $3d_{3/2}$ and $2p_{1/2}$ to $3d_{3/2}$ atomic states, respectively; these edges shift to higher energy for increasing iron oxidation state. In the spectrum, the main peak at 709.5 eV corresponds to Fe^{3+} species, while the lower intensity peak at 708.1 eV indicates the presence of Fe^{2+} in a smaller proportion [13-15]. The two structures at the L_2-edge centered at 721.3 eV and 722.7 eV verify the presence of Fe atoms in the Fe^{2+} and Fe^{3+} oxidation states; the L_2-edge and L_3-edge spin-orbit split of ~13 eV confirms the iron oxidation state. The synthesized Fe-carboxylate sample shows a higher amount of Fe^{3+}, i.e, the more stable oxidation state (electrons are more strongly bound to the nucleus than in the Fe^{2+} species [13]), indicating the synthesis of a pigment with color stability. The Co-carboxylate spectrum consists of a main peak centered at 778.5 eV splitting in three subpeaks along with a shoulder at 780 eV (Figure 3D). This line profile is similar to the spectrum reported to CoO, for which the peak split is associated with geometrical distortion of the crystal structure [5,6]. In this instance, as the NEXAFS line profile is nearly pared with the CoO NEXAFS, we suggest that in the Co-carboxylate, the Co^{2+} exists in an octahedral environment. For the Ni-carboxylate, the Ni L-edge indicated the presence of Ni^{2+} (Figure 3E) [5,6]. The peak centered at 931.6 eV in the Cu L-edge spectrum suggests the presence of mainly Cu atoms with oxidation state 2+, the low-intensity peak at 933.6 eV shows the presence of a low amount of Cu atoms with oxidation state 1+ [5,6].

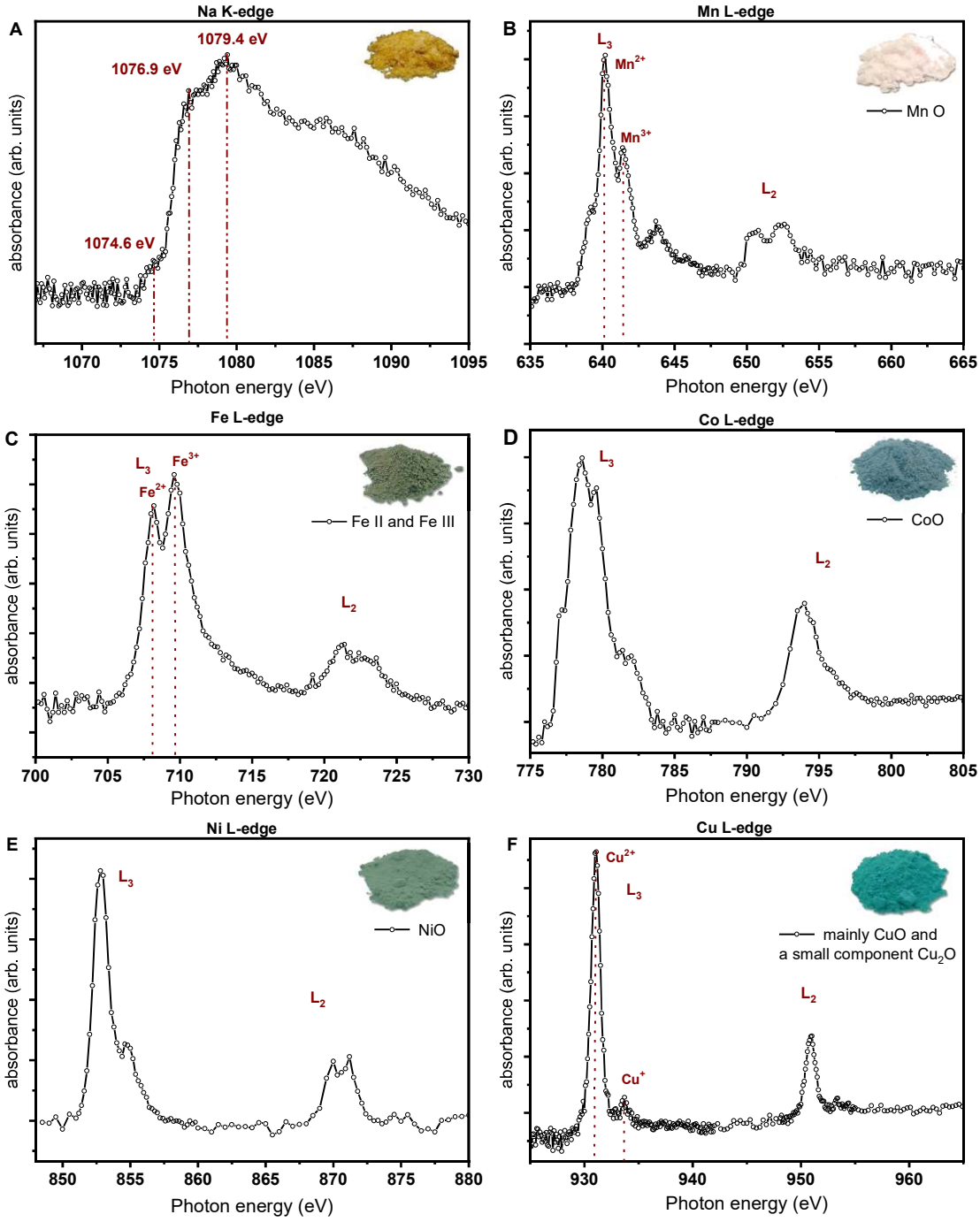

FIGURE 2. A) NEXAFS-TXM recorded on the Na-carboxylate sample. The Na K-edge indicates the incorporation of the Na atoms in the ionic form. B) NEXAFS-TXM recorded on the Mn-carboxylate sample. The Mn L-edge indicates the presence of Mn atoms with the 2+ and 3+ oxidation states. C) NEXAFS-TXM recorded on the Fe-carboxylate sample. The Fe L-edge suggests that Fe atoms have the 2+ and 3+ oxidation state. D) NEXAFS-TXM recorded on the Co carboxylate sample. The Co L-edge indicates the presence of Co atoms having the 2+ oxidation state. E) NEXAFS-TXM recorded on the Ni carboxylate sample. The Ni L-edge indicates the presence of Ni atoms with oxidation state 2+. F) NEXAFS-TXM recorded on the Cu carboxylate sample. Cu L-edge suggests the presence of copper mainly as Cu^{2+}, and the low-intensity component at 933.6 eV shows the presence of a low amount of Cu^{+}.

The antibacterial activity of the pigments was studied, too. Here we report on the Mn-abietate activity. The other complexes will be reported elsewhere. The antibacterial efficiency of Mn-abietate is shown in Table 2. An increase of the bacterial population to 6.86 log (CFU / cm2) was observed after 24h of incubation. Thus, the control (commercial paint) does not present antibacterial properties, and the inhibition potential can be attributed to the Mn-abietate. Mn-abietate, showed a good antibacterial potential against S. aureus presenting antibacterial activity values higher than 5 log reductions. The JIS Z 2801:2010 standard [8], considers that a material presents antibacterial activity when its value is ≥2 log reduction.

The mechanism of action of carboxylate complexes is not entirely elucidated. However, it is suggested that the lipophilic character of carboxylate favors the interaction with bacterial cells, resulting in membrane disruption, increasing membrane permeability, and causing bacterial cell death [16-19].

The antibacterial properties can be explained by the fact that manganese has antimicrobial activity reported in previous studies [20]. Pinus resin is mainly composed of abietic acid and its derivatives; the antibacterial properties of these acids are also reported in studies by Gu et al. [21] and Li et al. [22], justifying the results in table 2.

TABLE 2. The results of antibacterial activity against *S. Aureus*.

Sample	Total viable bacteria[a]	Antibacterial Activity [b]	Percentage of inhibition (%)[c]
Control	6.86±0.13	No effect	-
Paint 20% (Mn-abietate)	1.36±0.60	5.50 ±0.85	80.1749

[a] log UFC/cm^2 after 24h contact. [b] The antibacterial activity was determined by subtracting the average logarithm number of viable bacteria on control samples from the average logarithm number of viable bacteria treated with Mn-abietate after 24 h. Results are expressed as means and SD of three independent experiments (n=3) [c] Percentage of inhibition (%)=(B-C)/B×100), where B is the number of CFUs of the viable micro-organisms of the control sample. C is the number of CFUs for the test samples (10% and 20% Mn-abietate) after 24 h, respectively.

SUMMARY

In conclusion, we have shown that NEXAFS-TXM allows studying the electronic structure of dopants atoms in pigments at very low concentration. The number of photons per pixel was evaluated to be 3*10^7. The samples were stable during measurement. The analysis of the Na K-edge indicates the presence of only Na^+ íons in the Na-carboxylate sample. These ions are replaced by transition metal atoms resulting is pigments with different colors. The oxidation state of the carboxylates was identified by analysis of the L-edge recorded using NEXAFS-TXM.

ACKNOWLEDGEMENTS

We thank the Helmholtz-Zentrum Berlin for the allocation of synchrotron radiation beam time. J.C. thanks the FNRS for a mobility grant. C.B. is a Research Associate of the FRS-FNRS, Belgium. C.B. and J.C. thank the Belgian Fund for Scientific Research under the FRFC contract EQP 40002995 (PHOTOFUN).

REFERENCES

[1] M. Hassanpour, M. Salavati-Niasari, S.A.H. Tafreshi, H. Safardoust-Hojaghan, F. Hassanpour, "Synthesis, characterization and antibacterial activities of Ni/ZnO nanocomposites using bis(salicylaldehyde) complex precursor," Journal Alloys Compounds, vol. 788, pp. 383-390, 2019.

[2] Jamille S. Correa, Júlia O.Primo, CarlaBittencourt, Dienifer F.L.Horsth, Eduardo Radovanovic, Alceu T.Silveira-Jr, Henrique E.Toma, Cristina M. Zanette, Fauze J. Anaissi "Ecofriendly synthesis of Zn-abietate complex derived from Pinus elliottii resin and its application as an antibacterial pigment against S. aureus and E. coli", Dyes and Pigments,197, 109946, 2022

[3] A. Yildiz, M. Degirmencioglu, “Synthesis of silver abietate as an antibacterial agent for textile applications,” Bioinorganic Chemistry Applied, pp. 1-5, 2015.

[4] M. Berger, A. Roller, N. Maulide, “Synthesis and antimicrobial evaluation of novel analogues of dehydroabietic acid prepared by CH-Activation,” European Journal of Medicinal Chemistry, vol. 126, pp. 937-943, 2017.

[5] Frank de Groot, Akio Kotani, ‘Core Level Spectroscopy of Solids’ CRC Press

[6] Joachim Stohr NEXAFS Spectroscopy Springer

[7] P. Guttmann, C. Bittencourt, S. Rehbein, P. Umek, X. Ke, G.V. Tendeloo, C.P. Ewels, G. Schneider, “Nanoscale spectroscopy with polarized X-rays by NEXAFS-TXM,” Nature Photonics, vol. 6, pp. 25-29, 2012.

[8] E. Street, C. Lake, D. Koester, JIS Z 2801 : 2010 Antimicrobial Products – Test for Antimicrobial Activity and Efficacy, 60014 (2014) 1–4.

[9] P. Guttmann, et al., Microscopy and Microanalysis, 24 (S2) (2018), 202-203

[10] P. Guttmann, et al., Journal of Physics: Conference Series 186 (2009) 012064

[11] D.R. Neuville, L. Cormier, A.-M. Flank, R.J. Prado, P. Lagarde, “Na K-edges XANES spectra of minerals and glasses,” European Journal Mineralogy, vol. 16, pp. 809-816, 2004.

[12] C. Ragoen, L. Cormier, A.-I. Bidegaray, S. Vives, F. Henneman, N. Trcera, S. Godet, “A XANES investigation of the network-modified cation environment before and after the Na+/K+ ion-exchange in silicate glasses,” Journal of Non-Crystalline Solids, vol. 479, 2018.

[13] V. Drozd, G.Q. Liu, R. S. Liu, H.T. Kuo, C. H. Shen, D. S. Shy, X.K. Xing. “Synthesis electrochemical properties, and characterization of LiFePO4/C composite by a two-source method,” Journal of Alloys and Compounds, vol. 487, pp. 58-63, 2009.

[14] R.K. Hocking, E.C. Wasinger, Y.-L. Yan, F.M.F. de Groot, F.A. Walker, K.O. Hodgson, B. Hedman, E.I. Solomon, “Fe L-edge X-ray absorption spectroscopy of low-spin heme relative to non)heme Fe complexes: delocalization of Fe d-Electron into the Porphyrin Ligand,” Journal of the American Chemical Society, vol. 129, pp. 113-125, 2007.

[15] M. Giménez-Marqués, E. Bellido, T. Berthelot, T. Simón-Yarza, T. Hidalgo, R. Simón-Vázquez, Á. Gonzalez-Fernández, J.A.M.C. Asensio, R. Gref, P. Couvreur, C. Serre, P. Horcajada, “Graftfast surface engineering to improve MOF nanoparticles furtiveness, ” Small Journal, vol. 14, 2018.

[16] W. Gu, C. Qiao, S.F. Wang, Y. Hao, T.T. Miao, “Synthesis and biological evaluation of novel N-substituted 1H-dibenzo[a,c]carbazole derivatives of dehydroabietic acid as potential antimicrobial agents,” Bioorganic and Medicinal Chemistry Letters, vol. 24, pp.328–31, 2014.

[17] R.J. Kamble, P.V. Gaikward, “Peroxy titanium complex derived Fe-doped TiO2 Nanoparticles: Synthesis, properties and antibacterial activity,” Materials today: proceedings, vol. 45, pp. 3784-3788, 2021.

[18] V. Zelenák, K. Györyová, D. Mlynarcík, Antibacterial and antifungal activity of zinc(II) carboxylates with/without N-donor organic ligands, Met. Based. Drugs. 8 (2001) 269–274. https://doi.org/10.1155/MBD.2002.269.

[19] A. Turlybekuly, A.D. Pogrebnjak, L.F. Sukhodub, L.B. Sukhodub, A.S. Kistaubayeva, I.S. Savitskaya, D.H. Shokatayeva, O. V. Bondar, Z.K. Shaimardanov, S. V. Plotnikov, B.H. Shaimardanova, I. Digel, Synthesis, characterization, in vitro biocompatibility and antibacterial properties study of nanocomposite materials based on hydroxyapatite-biphasic ZnO micro- and nanoparticles embedded in Alginate matrix, Mater. Sci. Eng. C. 104 (2019) 109965. https://doi.org/10.1016/j.msec.2019.109965.

[20] S. Hajaria, H. Keypoura, M. T. Rezaeia, S. H. M. Faridab, R. W. Gablec. New 15-membered macrocyclic Schiff base ligand; synthesis some Cd(II), Mn(II) and Zn(II) complexes, crystal structure, cytotoxicity, antibacterial and antioxidant activity, J. Mol. Struct. 1251 (2022) 132049. https://doi.org/10.1016/j.molstruc.2021.132049

[21] W. Gu, C. Qiao, S.F. Wang, Y. Hao, T.T. Miao, Synthesis and biological evaluation of novel N-substituted 1H-dibenzo[a,c]carbazole derivatives of dehydroabietic acid as potential antimicrobial agents, Bioorganic Med. Chem. Lett. 24 (2014) 328–331. https://doi.org/10.1016/j.bmcl.2013.11.009.

[22] Z. Li, X. Yang, H. Liu, X. Yang, Y. Shan, X. Xu, S. Shang, Z. Song, Dual-functional antimicrobial coating based on a quaternary ammonium salt from rosin acid with in vitro and in vivo antimicrobial and antifouling properties, Chem. Eng. J. 374 (2019) 564–575. https://doi.org/10.1016/j.cej.2019.05.208.